Macromolecules

Article

pubs.acs.org/Macromolecules

Systematic Fluorination of P3HT: Synthesis of P(3HT-*co*-3H4FT)s by Direct Arylation Polymerization, Characterization, and Device Performance in OPVs

Patrick D. Homyak,[†] Yao Liu,[†] Jared D. Harris,[†] Feng Liu,[‡] Kenneth R. Carter,[†] Thomas P. Russell,[†,‡] and E. Bryan Coughlin*[,†]

[†]Department of Polymer Science & Engineering, University of Massachusetts Amherst, 120 Governors Drive, Amherst, Massachusetts 01003, United States

[‡]Materials Science Division, Lawrence Berkeley National Lab, 1 Cyclotron Road, Berkeley, California 94720, United States

Supporting Information

ABSTRACT: We present a strategy for tuning physical properties of P3HT-based copolymers by incorporating a fluorinated thiophene repeat unit. The synthesis and characterization of a series of fluorinated polythiophene P(3HT-*co*-3H4FT) materials are described, where the percentage of fluorinated repeat units in the polymer backbone is systematically varied from 0 to 100%. These P(3HT-*co*-3H4FT)s (**P0**, **P25**, **P50**, **P75**, and **P100**) were synthesized via direct arylation polymerization (DArP) methods. By varying the feed ratio of the two monomers, the percent of fluorinated repeat units (3H4FT) could be precisely controlled. As fluorination is increased, there is a strong effect on the electronic properties of the polymers, evidenced by a 0.4 eV drop in the E_{HOMO} level for **P100** when compared to **P0**. GIWAXS and TEM were used to determine the crystallinity and morphology. TEM analysis of thin film polymer/PCBM bulk-heterojunction blends indicates that increased fluorination does not result in stronger phase separation. Organic photovoltaic devices were fabricated to evaluate changes in device performance as a result of fluorination.

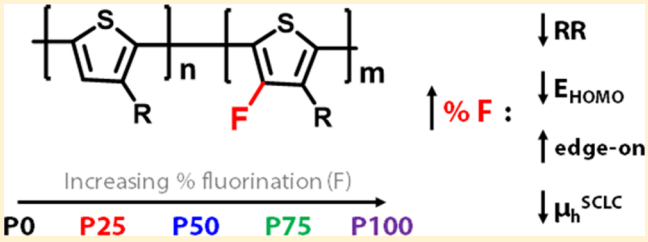

1. INTRODUCTION

Conjugated, semiconducting polymers have been an interesting research area due to their potential to serve as solution processable, active materials for a variety of organic electronic applications, such as organic photovoltaics (OPVs),[1−5] organic field-effect transistors (OFETs),[6] and organic light-emitting diodes (OLEDs).[7] Since these materials may be processed from solution, device fabrication can be achieved by roll-to-roll fabrication methods, ultimately leading to low-cost modules, particularly for large-area OPVs. Since devices can be fabricated on flexible, lightweight substrates, many niche solar power application areas can be served (e.g., remote locations, emergency scenarios, portable uses, short-term installations), in contrast to those typically served by conventional monocrystalline silicon solar panels (e.g., homes, permanent large-scale power arrays).

Poly(3-hexylthiophene) (P3HT) is the most well-known and studied conjugated polymer due to its availability, relative ease of synthesis, stability, good charge transport, and crystallinity.[8] In OPV devices, P3HT typically has power conversion efficiencies (PCEs) from 3 to 5%, depending on processing conditions, device architecture, and polymer molecular weight and dispersity.[8,9] Recently, a few reports have detailed the synthesis of modified P3HT materials, where fluorine atoms can be substituted in the 4-position of the 3-hexylthiophene (3HT) repeat unit (Scheme 1). The addition of fluorine as an electron-withdrawing substituent, due to its small van der Waals radius and high electronegativity, has proven to be an important tool for tuning physical and chemical properties of many conjugated polymers.[10,11]

Gohier et al. provided a monomer-modification approach for fluorinated polythiophenes, where a fluorinated terthiophene monomer was synthesized in five steps from 3-hexylthiophene (Scheme 1).[12] This monomer was then electropolymerized affording polythiophene films with ∼33% fluorination along the polymer backbone. Koo et al. demonstrated a two-step direct postpolymerization modification strategy,[13] where P3HT was first brominated, using an electrophilic brominating reagent (NBS). This produced 3H4BrT units in the polymer backbone that could then be lithiated with *n*-BuLi and quenched with an electrophilic fluorinating reagent (*N*-fluorobenzenesulfonamide) to produce fluorinated 3H4FT units in the polymer backbone. They were able to fluorinate 67% of the thiophene units in the polymer backbone. Recently, Fei et al. demonstrated that 100% fluorination could be achieved by a monomer-modification approach, where 2,5-dibromo-3-fluoro-4-hexylthiophene could be synthesized in four steps from either 3-hexylthiophene or 2,3,4,5-tetrabromothiophene and then

Received: February 22, 2016
Revised: March 31, 2016
Published: April 8, 2016

DOI: 10.1021/acs.macromol.6b00386
Macromolecules 2016, 49, 3028−3037

Scheme 1. Recent Synthetic Routes to Fluorinated Polythiophenes

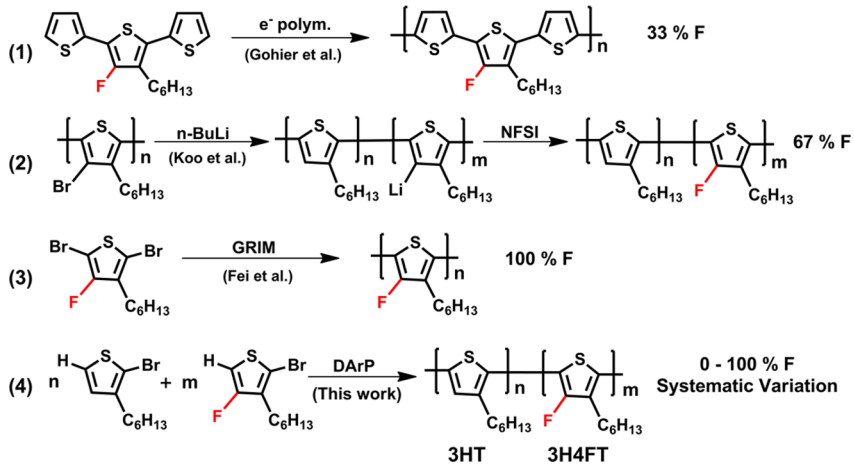

polymerized by Grignard metathesis (GRIM).[14] By this approach, different f-P3ATs were obtained where the length and branching of the alkyl (A) chain were varied from the original linear hexyl chain to influence the polymer solubility. Fluorination of P3HT was demonstrated to (1) lower the E_{HOMO} (increase IP), which should improve stability and theoretically increase open-circuit voltage (V_{oc}), (2) planarize the polymer backbone in the transoid configuration, while reducing long-range crystallinity, and (3) improve hole mobility in field-effect transistors.

Herein, we report the synthesis and properties for a series of P(3HT-*co*-3H4FT)s ranging from 0% to 100% fluorination. We used a monomer-modification approach along with direct arylation polymerization (DArP) techniques to demonstrate that the percent of fluorination in the copolymers can be precisely tuned by the monomer feed ratio. Thus, the properties of P3HT can be varied depending on the desired amount of fluorination. A few studies have demonstrated this approach with P3HT copolymers, incorporating thiophene monomers with modified side chains or functional groups.[15−18] This approach has also recently been demonstrated in fluorinated low bandgap donor−acceptor type conjugated polymers as well.[19−21] In our approach, DArP is enabled by the use of an A−B type monomer, containing both an active $C_{sp}{}^2$−H bond and an aryl bromide. Synthesis of P3HT by DArP has been thoroughly documented; however, this is the first example of fluorinated P3HT and copolymers synthesized by DArP.[17,22−31] Polymers containing 0%, 25%, 50%, 75%, and 100% of the fluorinated 3H4FT repeat unit, indicated by the nomenclature **P0**, **P25**, **P50**, **P75**, and **P100**, respectively, were synthesized. These materials were extensively evaluated to determine how fluorination influences light absorption, electronic properties, crystallinity, morphology, and performance in devices.

2. DISCUSSION

Modeling experiments were performed to understand the influence of fluorination on (1) the dihedral angle (twisting) along the polymer backbone and (2) the electronic properties of the polymers, in particular how the E_{HOMO} level is influenced by higher degrees of backbone fluorination. First, a thiophene dimer model was used to assess the relative energy of different conformational states, where the dihedral angle between the units was varied in 15° increments from 0° to ±180°, as shown in Figure 1 (here, 0° corresponds to a planar, anti, or trans conformation). Four models were considered, where the 4-

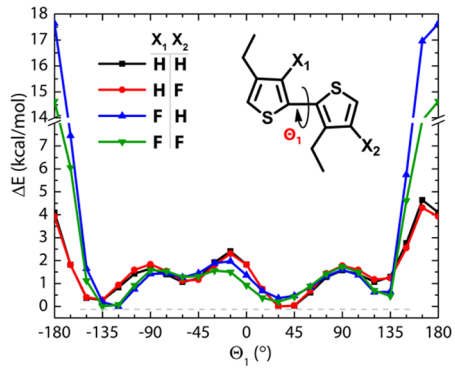

Figure 1. Change in relative energy, normalized to the lowest energy conformation, as a function of the dihedral (torsion) angle in a dimer thiophene model. $\Theta_1 = 0°$ is taken to be the planar anti confirmation (transoid). Potential energy for each conformation was calculated by DFT methods.

position functionality in the first (X_1) and second (X_2) units was systematically varied between H and F. Ethyl substituents were used in the 3-positions to reduce computational time. Density functional theory with the B3LYP functional and the 6-31G (d, p) basis set were used to calculate energies for each of the preset dihedral angles using Gaussian 09.[32] With this model, it becomes apparent that fluorine in the X_1 position greatly increases the rotational barrier around 180° (completely cisoid) versus the models where X_1 = H. This is due to the longer C−F bond (1.35 A) compared to a typical C−H bond (1.08 A) that creates greater steric repulsion or also greater electrostatic repulsion as a result of the increased electron density on the fluorine atoms relative to hydrogen. Additionally, with the use of an ethyl substituent for these models, the symmetry of the model is disturbed since the terminal methyl groups are out-of-plane relative to the conjugated thiophene. This slightly shifts and distorts the relative energy plot, where it is typically expected to have a perfectly symmetrical curve centered around 0°.[14,33]

Overall, each of the dimer models display both a local energy minima in an relatively transoid conformation (anti-gauche) with a dihedral angle of ∼35° and a second local energy minima in a relatively cisoid conformation (syn-gauche) at −135°. The

DOI: 10.1021/acs.macromol.6b00386
Macromolecules 2016, 49, 3028−3037

existence of two local energy minima is well documented in the polythiophene literature, and in most studies, an anti-gauche conformation is assumed.[33−35] Interestingly, when X_1 is fluorine, the global energy minima is around −135°, compared to when X_1 is hydrogen and the global energy minima is around 35°, as is more typically observed for thiophene-based polymers. This may indicate a slightly reduced preference for the fluorinated polymers to order into anti-gauche conformations, which may have implications on the crystallinity, as discussed later. In this dimer model, there does not appear to be enhanced planarity or a shift of the global energy minima toward 0° with the addition of the fluorine atoms in X_1 and X_2. This result may be limited by the use of a dimer model, which is known to underestimate rotational torsion barriers in comparison to longer oligothiophene models (where n = 10).[36] It is also interesting to note that the F,F dimer exhibits a lower relative energy (by ∼4 kcal/mol) in the fully cisoid conformation (180°) than the F,H dimer.

To understand the effect of increasing fluorination on the E_{HOMO} and E_g, tetramer models were studied (Figure 2). The

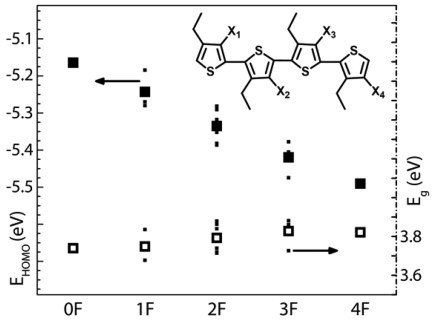

Figure 2. Calculated values for E_{HOMO} and E_g were obtained using DFT methods for 3-ethylthiophene tetramers with increasing fluorine substitution in the 4-position. Smaller dots represent individual calculations for tetramers where multiple possible isomeric sequences (e.g., **1F**, **2F**, and **3F**), while the larger symbols represent the average values.

models were built using the lowest relative energy dihedral angles obtained from Figure 1 as a starting point for geometric optimizations. The number of fluorine atoms substituted in the 4-position (X_1, X_2, X_3, X_4) of the thiophene tetramers was increased from 0 to 4, yielding five tetramer models: **0F**, **1F**, **2F**, **3F**, and **4F**. Thus, in the **1F** model, there is one fluorine substitution. In the **2F** model, there are two fluorine substitutions, and so forth. Each of these tetramers can be used as a comparison for the copolymers synthesized, as **1F** ≈ **P25**, **2F** ≈ **P50** ... **4F** ≈ **P100**. The same level of DFT theory was used as before to optimize system geometry (energy minimization) and calculate E_{HOMO} and E_{LUMO} (their difference estimated as E_g) for each tetramer. Since the **1F**, **2F**, and **3F** tetramers have multiple isomers depending on the unit sequencing (4, 6, and 4 isomers, respectively), calculations were performed for each possible isomeric sequence and each result is plotted in Figure 2 along with the overall average value. Tabulated results for each specific tetramer isomer are given in the Supporting Information (Table S1) along with representative structures of the models (Figures S1−S5).

The average E_{HOMO} values were calculated to be −5.16, −5.24, −5.34, −5.42, and −5.49 eV for the **0F**, **1F**, **2F**, **3F**, and **4F** models, respectively. It appears that the E_{HOMO} is systematically lowered (by ∼0.1 eV) with each fluorine substitution on the tetramer. Analysis of the E_g for the tetramer, calculated by subtracting the E_{LUMO} from the E_{HOMO}, suggests that the E_g is not strongly influenced by fluorination. Thus, the E_{LUMO} is reduced with increasing fluorination along with the E_{HOMO}. Overall, these computational results indicate that with increasing amounts of fluorination the E_{HOMO} is further lowered, which is beneficial for achieving higher V_{oc} in OPV devices, as well as greater oxidative stability. Thus, by systematically adjusting the percentage of fluorine in P(3HT-*co*-3H4FT)s, the molecular orbital energy levels may be precisely tuned.

For the synthesis of the P(3HT-*co*-3H4FT)s, direct arylation polymerization (DArP) was employed. Using a DArP strategy, statistical copolymers containing the 3HT and 3H4FT units can easily be achieved with the monobrominated **2Br3HT** and **2Br3H4FT** monomeric building blocks. These monomers have both an Aryl−Br and activated C−H functionality, making them suitable for DArP. P3HT has been previously synthesized by DArP, with good control over molecular weight, regioregularity (RR), dispersity, and branching.[23−25,27,28] Copolymers with precisely tuned amounts of the fluorinated repeat units (3H4FT) can be achieved by varying the ratio of the **2Br3H4FT** units in the polymerization feed ratio, thereby controlling the percentage of fluorine in the polymer backbone.

Synthesis of **2Br3H4FT** was achieved in one additional synthetic step from the known precursor 2,5-dibromo-3-hexyl-4-fluorothiophene.[12] Synthesis of this precursor is performed in a similar manner to the preparation of 2,5-dibromo-3,4-difluorothiophene,[37] except the initial starting material in this case is 3-hexylthiophene rather than thiophene. 2,5-Dibromo-3-hexyl-4-fluorothiophene was synthesized and shown to be a suitable monomer for polymerization by Grignard metathesis (GRIM) by Fei et al., affording fluorinated f-P3AT materials.[14] Here it was found that lithiation of this compound with *n*-BuLi occurs selectively in the 5-position due to the presence of the strong electron-withdrawing fluorine group in the adjacent 4-position. Quenching of the lithiated thiophene intermediate with water affords the desired **2Br3H4FT** monomer as a single product (Scheme 2). ^{1}H and ^{19}F NMR confirmed the

Scheme 2. Synthesis of 2Br3H4FT Monomer for DArP

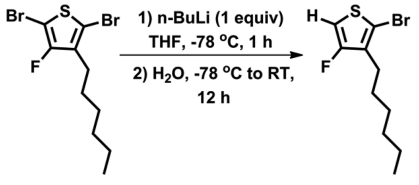

2Br3H4FT (59 %)

formation of a single product. No lithiation of the 2-position was observed. A similar directing effect due to the electronegative fluorine in the 4-position was observed by Heeney, when 2,5-dibromo-3-hexyl-4-fluorothiophene was used to generate a Grignard reagent for GRIM.[14]

With this monomer, statistical copolymers with finely tuned amounts of fluorination along the conjugated backbone could be achieved by varying the **2Br3H4FT**:**2Br3HT** feed ratio (Scheme 3). Five copolymer compositions were targeted with 0, 25, 50, 75, and 100% of the fluorinated monomer (by molar ratio), which correspond to **P0**, **P25**, **P50**, **P75**, and **P100**, respectively. Conditions for DArP were first optimized for the

DOI: 10.1021/acs.macromol.6b00386
Macromolecules 2016, 49, 3028−3037

Scheme 3. Synthesis of P0−P100 Copolymers by DArP

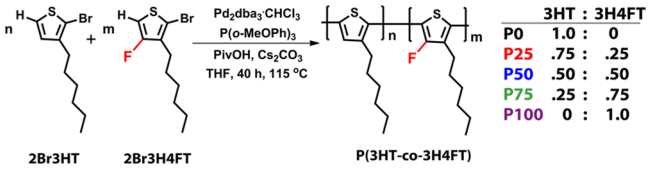

synthesis of **P0** and then applied to the rest of the copolymer series resulting in high molecular weight polymers (Table 1). In

Table 1. Molecular Weight, Regioregularity, and Composition of P(3HT-*co*-3H4FT)s

	M_n[a] [kg/mol]	M_w[a] [kg/mol]	$Đ$	RR[b] [%]	F[c] [%]
P0	13.0	18.2	1.4	95	0
P25	12.9	17.8	1.4	89	27
P50	16.4	32.5	2.0	85	50
P75	12.4	20.2	1.6	81	75
P100	5.6	6.9	1.2	78	100

[a]Measured by GPC versus polystyrene standards in 1,2,4-trichlorobenzene at 135 °C (1 mg/mL). [b]Regioregularity (RR) estimated by ^{1}H NMR. [c]Corresponds to percent of 3H4FT repeat units in final polymer, measured by ^{1}H NMR.

accordance with our previous experience, $Pd_2(dba)_3{\cdot}CHCl_3$ and tris(*o*-methoxylphenyl)phosphine were selected as the Pd^0 source and ligand. Cs_2CO_3 (3 equiv) was used as an insoluble heterogeneous base source, generating soluble cesium pivalate *in situ* from pivalic acid (1 equiv). Optimization revealed THF to be the most effective solvent for the polymerizations.

Number-average molecular weights (M_n) for **P0**, **P25**, **P50**, and **P75** were similar, 12−16 kg/mol as measured by high-temperature GPC. For **P100** lower molecular weight materials, ∼5.6 kg/mol was achieved. Qualitative observations indicate that this is presumably due to the reduced solubility of **P100** in the polymerization solvent versus the less fluorinated copolymers **P0**−**P75**. Dispersities for the polymers were within a reasonable range (<2) given the step-growth nature of the polymerization. Regioregularity (RR) of the polymers and the percentage of fluorinated repeat units were estimated by ^{1}H NMR.

By ^{1}H NMR, the composition of the polymers can be clearly verified. In the region from δ 2.5−3.0 ppm (Figure 3) the α-CH_2 peak for the 3HT repeat units can be observed at δ 2.83 ppm while the α-CH_2 peak for the 3H4FT repeat units is shifted to δ 2.76 ppm, clearly demonstrating the incorporation of the 3H4FT unit in the copolymers. Although fluorine is an electron withdrawing group inductively, resonance donating of the extra lone-pair electrons dominates, leading to an upfield shift of the α-CH_2 peak observed in NMR. The peak at δ 2.76 ppm clearly increases as higher percentages of the fluorinated 3H4FT unit are incorporated into the polymer, accompanied by equal decreases in the 3HT peak at δ 2.83 ppm. Full NMR (^{1}H and ^{19}F) spectra are provided in the Supporting Information. Following the recent report by Koo et al., the copolymer composition (%F) was estimated by comparing the integration value of the aromatic thiophene 4-H peak at $\delta \sim 7.0$ ppm and the sum of the integration values for the α-CH_2 peaks over the range of $\delta \sim$ 2.5−2.9 ppm (Table 1).[13] From this analysis, it appears that the final polymer composition was quite comparable to the targeted compositions determined by the monomer feed ratio. Furthermore, ^{19}F NMR (Supporting

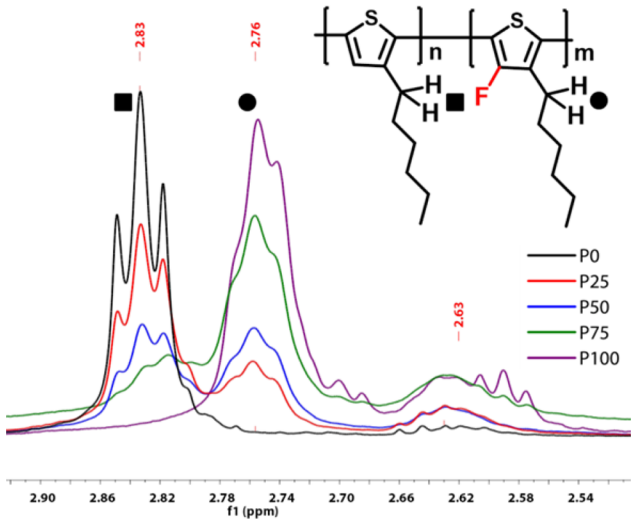

Figure 3. ^{1}H NMR for **P0**−**P100**. The α-CH_2− on the hexyl side chain can be used to differentiate between the two monomer units. Peaks at δ 2.83 and 2.76 ppm correspond to the α-CH_2 on 3HT (■) and 3H4FT (●) units, respectively. Peaks resulting from head-to-head couplings can be seen around δ 2.6 ppm.

Information) suggests the formation of statistical copolymers, as opposed to blocky or alternating structures, since a distribution of many peaks of similar intensity are observed in the **P50** case, which resembles previous observations in P3HT-based copolymers.[38,39]

Head-to-head couplings, from both 3HT and 3H4FT units, can be observed at $\delta \sim$ 2.63 ppm, as has been previously demonstrated for P3HT.[40] Integration of these peaks allows for RR to be calculated for each copolymer (Table 1). As the content of the 3H4FT monomer is increased, a corresponding decrease in RR is observed. The highest RR is observed for **P0** (95%), whereas the lowest is observed for **P100** (78%). The decreased RR is likely due to differences in monomer reactivity, resulting from the altered electronic character of the **2Br3H4FT** monomer versus the **2Br3HT** monomer. Typically head-to-head homocouplings in DArP can be suppressed by the use of optimized polymerization conditions, bulky carboxylate sources, and phosphine ligands.[28,41] Phosphine ligands create a larger coordination sphere around the Pd center, inhibiting Pd dimer formation and the subsequent disproportionation that leads to homocouplings. In this case it not clear what the reason is for the reduced RR, since each polymer was synthesized under identical polymerization conditions.

MALDI-TOF mass spectrometry was used as an additional characterization aid for studying the structure of these copolymers (Figure 4). In the homopolymers, **P0** and **P100**, narrow periodic peaks can be observed. The spacing between the peaks corresponds to the repeat unit molecular weights, and the absolute molecular weights indicate exclusively H/H termination. Full MALDI-TOF spectra are provided in the Supporting Information. Additional peaks in the **P0** and **P100** spectra indicate some loss of $-C_5H_{11}$ (71 amu) fragments, and Br (78 amu) in the case of **P100**, as observed previously.[42] As the polymer composition is varied from **P0** to **P25**, a broadening of the peak distribution from a single peak to several peaks clustered in a normal distribution can be observed in the MALDI spectrum. This is expected due to the statistical distribution of possible copolymer compositions, with an average of 25% of the 3H4FT repeat unit. While the copolymer

DOI: 10.1021/acs.macromol.6b00386
Macromolecules 2016, 49, 3028−3037

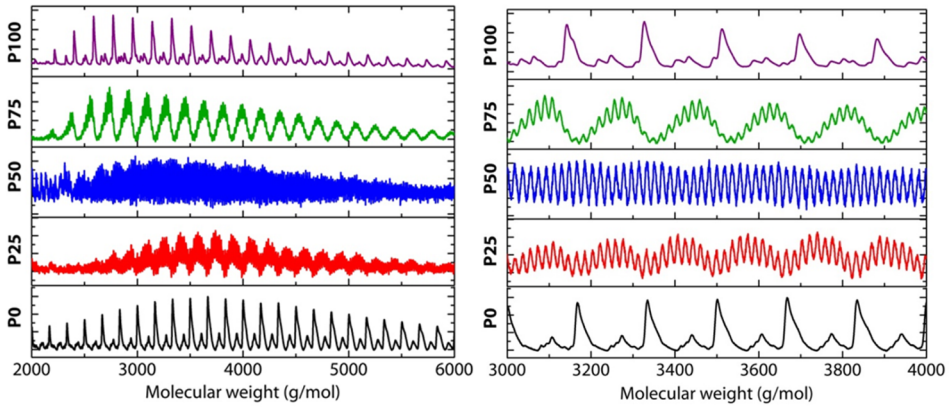

Figure 4. MALDI-TOF mass spectra for **P0**–**P100**: full spectra (left) and 3000–4000 g/mol inset (right). *Y*-axis is intensity (counts).

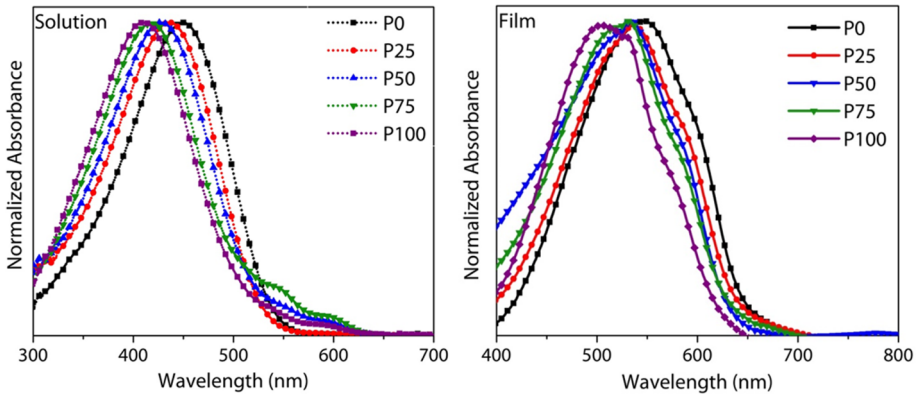

Figure 5. UV–vis absorption of **P0**–**P100** copolymers in heated (50–55 °C) $CHCl_3$ (left) and in solid thin films (right) cast from $CHCl_3$.

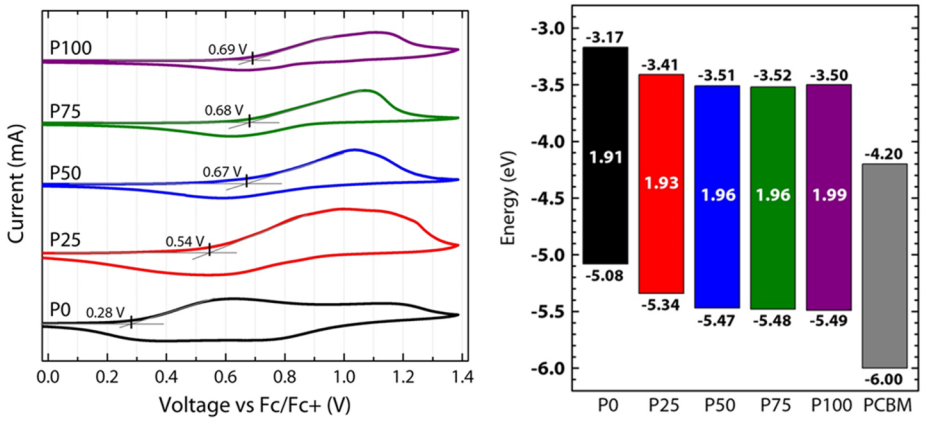

Figure 6. Measurement of onset of oxidation (i.e., E_{HOMO}) by cyclic voltammetry of polymer films (left). Films were cast directly on the electrode from polymer solutions in $CHCl_3$; potentials were standardized using an external ferrocene (Fc/Fc^+) reference. (right) Band energy diagrams with E_{HOMO}^{CV}, E_{LUMO}, and E_g^{UV-vis} for **P0**–**P100**, as compared to PCBM ($E_{LUMO} = E_g^{UV-vis} - E_{HOMO}^{CV}$).

composition in the case of **P25** will have an aggregate average of 25% 3H4FT units, individual chains will vary in their monomer ratios, resulting in the observed peak broadening. This effect is amplified for **P50** where all the peaks appear to be nearly equal in intensity, separated by a mass of 19 amu (i.e., the mass of fluorine). In **P75**, the peak distribution is more similar to that of **P25**, as expected. Overall, these results provide a second method of verifying both copolymer structure and composition.

Optical properties of the copolymers in solution and solid films were studied by UV–vis spectroscopy (Figure 5). In solution, **P0** has a maximum absorption at ∼460 nm. With increasing fluorination, the λ_{max} is steadily blue-shifted with **P100** exhibiting maximum absorption at ∼410 nm. Lower energy shoulder absorption (∼550 nm) in the **P50**–**P100** copolymers is indicative of these materials' tendency to aggregate in solution. Fluorination is known to enhance C–H···C–F interactions in aromatic molecules, which can lead increased aggregation in solution and reduced solubility.[14,19,43]

In thin-film absorption, each of the copolymers demonstrated enhanced absorption at longer wavelengths. This is due to π–π orbital overlap as the copolymers crystallize into well-

DOI: 10.1021/acs.macromol.6b00386
Macromolecules 2016, 49, 3028–3037

ordered structures. The onset of absorption indicates the lowest energy photons that may be absorbed (i.e., the bandgap) for each of the materials. **P0** has an onset of absorption of ∼650 nm, corresponding to a bandgap of 1.91 eV. With increasing fluorination, the absorption onset shifts to shorter wavelengths, as with the solution spectra, leading to slightly increased bandgaps of 1.93, 1.96, 1.96, and 1.99 eV in **P25**, **P50**, **P75**, and **P100**, respectively. Slightly blue-shifted absorption in fluorinated thiophene oligomers and polymers has been observed previously[12−14] as well as in many examples of various fluorinated conjugated polymers.[10,11]

Measurement of the onset of oxidation (i.e., E_{HOMO}) for each of the copolymers was achieved using cyclic voltammetry (Figure 6). With a systematic increase in the amount of fluorination, it would be expected that the onset of oxidation steadily increases in a somewhat linear manner as indicated by computational results for these systems. However, what is empirically observed is quite different. **P0** exhibits an onset of oxidation at 0.28 V. With 25% fluorination in **P25** the onset of oxidation is increased by ∼0.26 to 0.54 V. In **P50**, the onset of oxidation is again increased by ∼0.13 to 0.67 V. At this point, despite increasing fluorination, the onset of oxidation seems to hit a plateau value and does not increase any further. **P75** and **P100** thus display similar onsets around 0.69 V. This observation can be thought of as resembling the classic donor−acceptor copolymer paradigm, where the "donor" unit is the major contributor to the overall E_{HOMO} and the "acceptor" is the major contributor to the E_{LUMO}.[2] In this case, once the copolymer ratio reaches 50% (**P50**), the polymer can be visualized as quasi-alternating, and thus the E_{HOMO} level is "pinned" at that level. When the amount of 3H4FT units ("donor" units) is increased further to 75% and 100%, the E_{HOMO} then remains unchanged since this unit is the major contributor toward the observed E_{HOMO}. As a verification of the cyclic voltammetry results, ultraviolet photoelectron spectroscopy (UPS) experiments were also performed. Comparable results were obtained for the E_{HOMO} levels as measured by UPS (Supporting Information).

Overall, the E_{HOMO} for the copolymers ranges from −5.08 eV for **P0** to −5.49 eV in **P100**, as displayed in Figure 6. Thus, fluorine substitution can dramatically lower the E_{HOMO} by ∼0.4 eV, which is more significant than many examples of fluorinated conjugated polymers where smaller shifts of 0.1−0.2 eV are typically observed.[10,44] Recent reports of f-P3ATs show similar shifts in the E_{HOMO} as observed here.[14] The capability to adjust the E_{HOMO} over a range of 0.4 eV can be useful for tuning exact energy levels for optimum energy level alignment, improved V_{oc}, and better charge separation.

The crystalline ordering of each copolymer, both in pure polymer films and in polymer:PCBM blend films, was investigated by grazing incidence wide-angle X-ray scattering (GIWAXS) (Figure 7). In the pure polymer films, peaks corresponding to the interchain lamellar spacings (100), (200), and (300) can be clearly observed in the out-of-plane (q_z) direction, indicating a primarily edge-on crystal orientation. As fluorine content is increased, the intensity of the (200) and (300) peaks decreases, suggesting a decrease in the periodic order of the crystalline domains, and an overall reduction in the crystallinity in pure polymer films. The position of the peak (∼0.4 Å^{-1}) remains unchanged, as expected, since this *d*-spacing is dominated by the length of the alkyl side chains (−C_6H_{13}). The prominence of the (010) peak at ∼1.6 Å^{-1} in the in-plane (q_{xy}) direction indicates again that the $\pi-\pi$ stacking and the overall crystallite orientation is primarily edge-on.

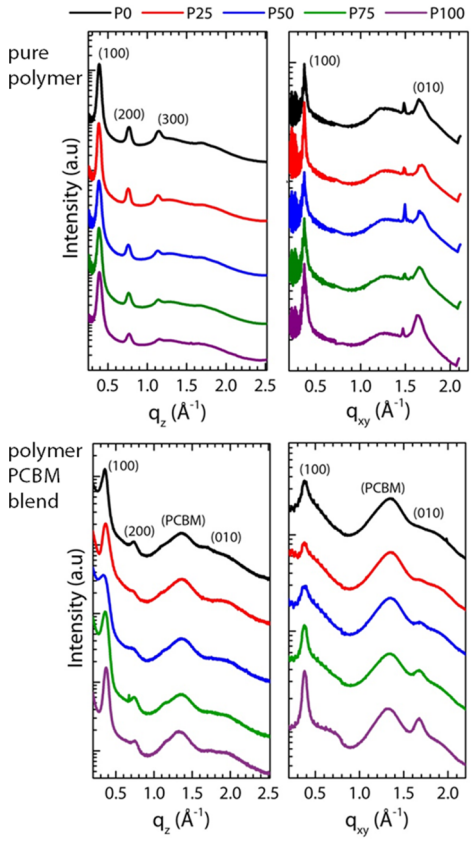

Figure 7. GIWAXS scattering out-of-plane (left) and in-plane (right) line cuts for pure polymer thin films (top) and polymer:PCBM blend active layer films (bottom).

In the blended thin films with the acceptor material ($PC_{71}BM$) used for the OPV device active layers, the polymers display subtle differences compared to the pure polymer films. First, along q_z and q_{xy}, the intensity of the (100) reflection decreases with increasing fluorine content (up to **P50**). With increasing fluorine content beyond **P50**, the reflection sharpens and intensifies up to **P100**. This suggests that crystalline order in the blends is decreased as the structural order in the copolymer backbone has more variation, with **P50** showing the least crystallinity, followed by **P25** and **P75**, which show similar order. Since a well-defined repeat unit structure in polymers is known to enhance crystallinity, this is not particularly surprising. Most notable in the in-plane (q_{xy}) scattering is the appearance of a significant (010) peak with increasing fluorine content. The (010) peak in the **P0** blend is almost nonexistent, but from **P25** up to **P100**, the (010) increases steadily as fluorine content is increased with no change in the $\pi-\pi$ stacking distance. The increasing intensity of the (010) peak with increasing fluorination indicates that the molecular ordering of the polymers is preferentially adopting an edge-on orientation relative to the substrate, which is particularly enhanced in the presence of PCBM. However, the increased intensity in the (010) does not necessarily correlate to increased crystallinity overall.

OPV devices were fabricated to evaluate potential trends in V_{oc} with the observed E_{HOMO} levels from CV and determine if increased fluorination offers any performance advantage. OPVs were constructed with a standard architecture (ITO/

DOI: 10.1021/acs.macromol.6b00386
Macromolecules 2016, 49, 3028−3037

PEDOT:PSS/polymer:$PC_{71}BM$/Ca/Al), where the active layer was spin-coated from *o*-DCB. Representative current−voltage curves are provided in Figure 8, and averaged device characteristics are given in Table 2. Reliable devices could not be fabricated using **P100** due to reduced solubility, which led to the formation of extremely rough films. For **P25** and **P50**, the V_{oc} is enhanced relative to **P0**. This shift corresponds with the lower E_{HOMO} for these materials; however, this trend does not follow through the series as **P75** does not show a higher V_{oc}. Higher V_{oc} can typically be correlated to larger $E_{HOMO}^{donor} - E_{LUMO}^{acceptor}$ offsets.[45] However, V_{oc} is also known to decrease with increased recombination at the either the donor/acceptor bulk heterojunction interface or interlayer interface, which may be the case for **P75**, due to slight differences in polymer solubility and/or greater immiscibility with PCBM.[45]

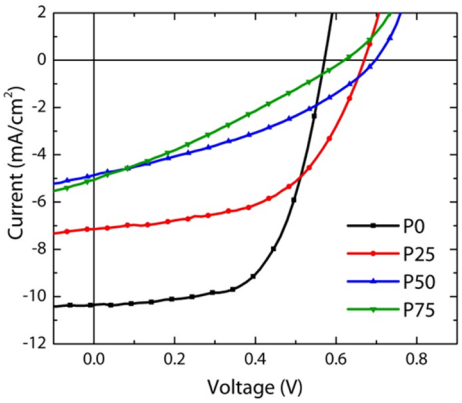

Figure 8. Representative current density−voltage characteristics of polymer:$PC_{71}BM$ bulk heterojunction OPV devices measured under AM1.5G irradiation.

With increasing fluorination, the short-circuit current (J_{sc}) and fill factor (FF) seem to be systematically reduced, possibly due to decreased crystallinity and/or increasing edge-on orientation as evidenced by GIWAXS. Reduced J_{sc} could also be a result of the decreasing RR that was observed in the increasingly fluorinated materials by NMR, which is known to influence hole mobility in polythiophenes. Lower FF may suggest a greater surface roughness of the active layer films and subsequently poorer interlayer/electrode contact, which could be the result of the slight differences in solubility with increasing fluorination. FF is also heavily influenced by balanced charge transport between the donor/acceptor materials, and so reduced polymer hole-mobility could also reduce FF. Overall, a PCE of 3.6% for **P0** corresponds well to published reports for the P3HT:$PC_{71}BM$ system, indicating that the DArP method used for this study can produce high quality materials.[8] However, analysis of the PCE for **P25**−**P75** indicates that increased fluorination is detrimental to the device performance overall.

Hole mobilities (Table 2) were estimated using space charge limited current (SCLC) techniques with hole-only devices measured in the dark. *J*−*V* curves are provided in the Supporting Information. The highest hole mobility was observed in **P0** (9.7×10^{-4} cm^2 V^{-1} s^{-1}), and as the percent fluorination was increased, hole mobility steadily decreased to the lowest observed mobility in **P75**. These measurements (for **P0**) are consistent with previous hole-mobility measurements for P3HT synthesized by DArP as measured by SCLC methods.[17,23,46] The decreasing trend in SCLC mobilities mirrors the decreasing trend observed in the J_{sc} for OPV devices. Given the similar molecular weights of the polymers, it is likely that lower mobility as fluorination is increased is related to the lower regioregularity in those materials, as well as differences in crystallinity.

In previous studies of fluorinated polymers, it has been shown that fluorination can markedly influence the morphology during spin coating.[43,44] The addition of fluorine can impart changes in solubility, surface segregation, or also induce a fluorophobicity effect with the acceptor, PCBM, creating phase separated blends with features that are too large (>100 nm) for efficient exciton transport and dissociation. Often this issue requires fine-tuning the spin-coating solvent using binary solvent mixtures or additives to ensure formation of the appropriate morphology. Thus, it is important to understand the blend morphology in this system, where the percent fluorination is varied over a large range. As evidenced by TEM (Figure 9), regardless of the percent fluorination, well mixed bulk-heterojunction morphologies were formed, showing no significant change in the morphology. This indicates that the observed device performance is not limited by a large scale phase separation. Furthermore, since solvent additives are often employed to reduce immiscibility/phase separation, their use in this case would not necessarily lead to any obvious benefits. While each of the blends appears to form well dispersed bulk-heterojunction domains, as fluorination is increased, a slight coarsening of the features can be observed, possibly indicating a change in the domain purity that provides the observed contrast enhancement. In the **P100** image, clear variations in the film thickness can be observed. This is due to the poor solubility of **P100**, causing it to prematurely aggregate and precipitate during spin-coating. The TEM results suggest that the bulk-heterojunction morphology is not the limiting factor for device performance and that differences in polymer regioregularity and crystallinity might be the origin of the reduced device performances as fluorination is increased.

3. CONCLUSION

A series of P3HT-based copolymers were synthesized by direct arylation polymerization (DArP) techniques. By varying the

Table 2. Photovoltaic Characteristics of Polymer:$PC_{71}BM$ OPV Devices

	V_{oc} [V]	J_{sc} [mA/cm²]	FF [%]	PCE [%]	μ_h[c] [cm^2 V^{-1} s^{-1}]
P0	0.57 ± 0.01	10.42 ± 0.07	60.55 ± 1.72	3.60 ± 0.10	9.7×10^{-4}
P25	0.67 ± 0.01	7.20 ± 0.05	50.94 ± 2.49	2.44 ± 0.12	1.9×10^{-4}
P50	0.70 ± 0.01	4.72 ± 0.20	36.85 ± 0.45	1.21 ± 0.04	3.9×10^{-5}
P75	0.61 ± 0.00	4.80 ± 1.15	28.11 ± 0.96	0.82 ± 0.18	2.2×10^{-5}

[a]Measurements represent average ± standard deviation for >4 devices. [b]All active layer films processed from DCB. [c]Hole mobility measured by SCLC methods.

DOI: 10.1021/acs.macromol.6b00386
Macromolecules 2016, 49, 3028−3037

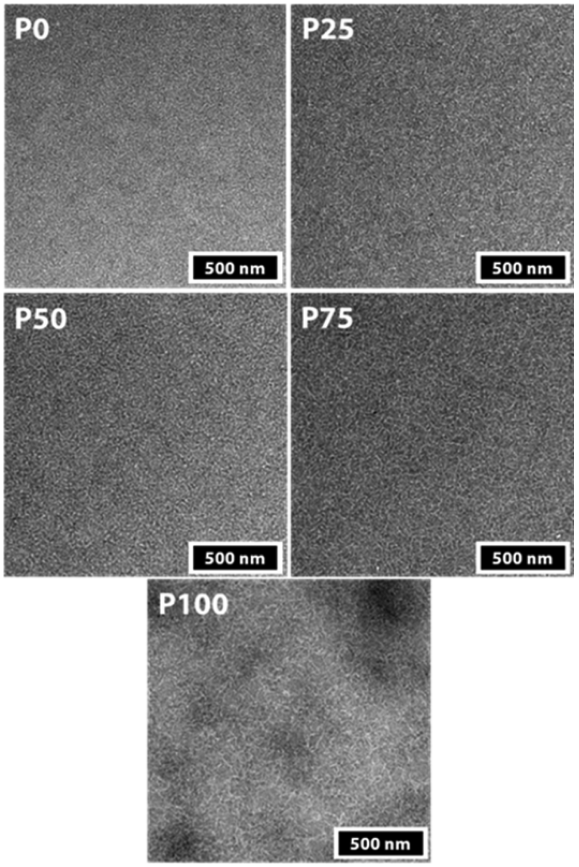

Figure 9. TEM images of the polymer:PCBM active layer blends. Films were prepared in a manner consistent with the preparation of the OPV device active layers. Scale bar is 500 nm for all images.

feed ratio of the two monomers, one fluorinated (**2Br3H4FT**) and one non-fluorinated (**2Br3HT**), the percentage of each monomer repeat unit in the polymer backbone, and thus the percent fluorination, could be tuned from 0 to 100%. NMR evidence confirms that the repeat unit ratios in the copolymers are nearly identical to the feed ratios and that increasing fluorination is accompanied by a concurrent decrease in the regioregularity. Investigation of the electronic properties of these materials shows that as the percent fluorination is increased, the E_{HOMO} is lowered from −5.08 eV for **P0** to −5.47 eV for **P50**. DFT calculations support this trend. Experimental results indicate that only 50% fluorination is required to reach the lowest attainable E_{HOMO} level for these copolymers, which would provide the maximum benefit for enhancing the V_{oc}. GIWAXS results suggest that increasing fluorination leads to an increasingly edge-on polymer orientation in bulk-heterojunction blends but does not indicate any major differences in the crystalline lattice dimensions. Devices were fabricated to measure OPV performance and SCLC mobility. **P0** (P3HT) has a PCE of 3.6%, which is consistent with previous reports for systems of this type. Generally, as fluorination was increased, the performance of OPVs suffered, with decreases in the J_{sc} and FF values. This was mirrored in the observed mobility by SCLC where **P0** had the highest mobility (9.7×10^{-4} cm^2 V^{-1} s^{-1}) and increasing fluorination lowered the mobility consistently to 2.2×10^{-5} cm^2 V^{-1} s^{-1} in **P100**. TEM images suggest that fluorination does not greatly affect the sizing of the domains in the bulk-heterojunction morphology. Overall, we have reported a synthetic approach for tuning the properties of P3HT-based copolymers utilizing DArP techniques. While modifications to P3HT did not lead to enhanced device performance, the synthetic approach presented represents an interesting route to tailor the properties of P3HT by incorporating small amounts of functionalized monomers.

4. EXPERIMENTAL SECTION

4.1. Materials. All reagents and chemicals were purchased from commercial sources (Matrix Scientific, Sigma-Aldrich, Acros Organics, Alfa Aesar) and used without further purification unless stated otherwise. 2-Bromo-3-hexylthiophene (**2Br3HT**) and 3-hexylthiophene were purchased from Sigma-Aldrich. The precursor to 2-bromo-3-hexyl-4-fluorothiophene (**2Br3H4FT**) and 2,5-dibromo-3-hexyl-4-fluorothiophene was synthesized by previously demonstrated synthetic procedures.[12,14,37] All reactions were performed under an inert (N_2) atmosphere.

4.2. Characterization. ^{1}H and ^{19}F NMR spectra were collected with a 500 MHz Bruker Ascend instrument with variable temperature capability. UV−vis absorption measurements of polymer solutions and films were performed on a PerkinElmer Lamba 25 UV−vis spectrometer. Solution spectra were measured from dilute polymer solutions in $CHCl_3$ at elevated temperatures to reduce aggregation. Films for absorption spectra were spin-coated from 10 mg/mL polymer solutions in $CHCl_3$ at 1500 rpm for 60 s. Polymer molecular weight and dispersity ($Đ$) analysis was completed via gel-permeation chromatography (GPC) in 1,2,4-trichlorobenzene at 135 °C using a Polymer Laboratories PL-220 high- temperature GPC instrument calibrated against polystyrene standards. MALDI-TOF experiments were performed on a Bruker microflex instrument, using DCTB (trans-2-[3-(4-*tert*-butylphenyl)-2-methyl-2-propenylidene]-malononitrile) as the ionizing matrix (1:1000 w/w polymer to matrix). Cyclic voltammetry (CV) measurements of the polymer films were done with a Bioanalytical Systems Inc. (BASi) EC Epsilon potentiostat using a three-electrode configuration consisting of a glassy carbon working electrode, a $Ag/AgNO_3$ (0.01 M in acetonitrile) reference electrode, and a Pt wire counter electrode with tetrabutylammonium hexafluorophosphate (0.1 M) in acetonitrile as the electrolyte solution. Measurements were calibrated to the ferrocene/ferrocenium redox couple (Fc/Fc^+) with an external reference. Films for CV were drop-cast directly onto the glassy carbon working electrode from polymer solutions in $CHCl_3$. Bright-field TEM was conducted using a JEOL 2000 FX TEM instrument operating at an accelerating voltage of 200 kV. Active layer films for TEM were spin-coated in the same manner as for OPV devices on PEDOT:PSS. The sample films were then floated onto copper TEM grids in water. Molecular modeling was performed using the Gaussian 09 suite of programs.[32]

4.3. Synthesis of 2-Bromo-3-hexyl-4-fluorothiophene (2Br3H4FT). Into a dry 1 L round-bottom flask was added 2,5-dibromo-3-hexyl-4-fluorothiophene (13.75 g, 39.96 mmol) and 400 mL of anhydrous THF (0.1 M) under the protection of dry N_2(g). The mixture was cooled to −78 °C in a dry ice/acetone bath. *n*-BuLi (16.3 mL, 2.5 M, 1.02 equiv) was added dropwise over 30 min, during this time the color changed from clear and colorless, to dark blue-green before ultimately turning orange, indicating the formation of the lithiated intermediate. The reaction was stirred at −78 °C for 30 min. Water (12 mL) was then added dropwise to quench the lithiated intermediate, and the mixture became yellow with white precipitate. After warming to RT overnight, the reaction mixture was washed with water, extracted with ether, washed with brine, dried with $MgSO_4$, and concentrated yielding an orange oil. The crude product was purified by column chromatography on SiO_2 (hexanes), vacuum distillation, and finally by reverse phase (C18) column chromatography (hexanes) to isolate the pure product **2Br3H4FT** as a clear oil (6.25 g, 23.57 mmol, 59%). Only one isomer was observed, indicating a selective reaction. ^{1}H NMR (500 MHz, $CDCl_3$): 6.62 (1 H, d, J = 1.5 Hz), 2.51 (2 H, t, J = 7.5 Hz), 1.53 (2 H, m), 1.30 (6 H, m), 0.88 (3 H, m). ^{19}F NMR (470.385 MHz, CD_2Cl_2): −126.22. GC-MS (m/z): Found: 264, 266 g/mol (Calcd: 263.998, 265.996 for [$C_{10}H_{14}BrFS$]).

DOI: 10.1021/acs.macromol.6b00386
Macromolecules 2016, 49, 3028−3037

4.4. Typical Polymerization Procedure. All polymers were synthesized using the same optimized DArP procedure. Provided is a typical polymerization procedure used in this work. Into a 10 mL Schlenk tube was added **2Br3HT** and **2Br3H4FT** in the appropriate molar feed ratio at 3 mmol total monomer scale, 62.1 mg of $Pd_2dba_3CHCl_3$ (0.06 mmol, 0.02 equiv), 84.57 mg of P(*o*-MePh)$_3$ (0.24 mmol, 0.08 equiv), 306 mg of PivOH (3 mmol, 1 equiv), and 2.932 g of Cs_2CO_3 (9 mmol, 3 equiv), followed by purging with N_2. THF (6 mL, 0.5 M) was then added as solvent, and air was removed via three freeze−pump−thaw cycles. The Schlenk tube was then securely sealed with a Teflon stopper, enabling superheated temperatures. The reaction mixture was stirred at RT for 20 min and then heated to 115 °C for 40 h. After completion of the reaction time, the contents of the reaction vessel were then cooled and precipitated into stirring methanol. $CHCl_3$ was used to dissolve any solid material prior to precipitation. All precipitated solids were then collected by filtration and purified by Soxhlet extraction washing with methanol, acetone, and hexanes. The polymers were then extracted with $CHCl_3$, precipitated into stirring MeOH, filtered, and dried. To ensure thorough removal of Pd from the samples, each of the polymers was redissolved in $CHCl_3$, stirred with diethylammonium diethyldithiocarbamate for 6 h, and reprecipitated into MeOH. ^{1}H and ^{19}F NMR spectra along with MALDI-TOF mass spectra are provided for each of the polymers in the Supporting Information.

4.5. OPV Device Preparation. Standard device architecture (ITO/PEDOT:PSS/active layer/Ca/Al) was used. Indium tin oxide (ITO)-coated glass substrates (20 ± 5 ohms/square) were purchased from Thin Film Devices Inc. Substrates were cleaned through ultrasonic treatment in detergent, water (2×), acetone, and isopropyl alcohol and dried in an oven overnight. The ITO substrates were then cleaned by ultraviolet ozone treatment (15 min), and PEDOT:PSS (Clevios P VP A1 4083) was then spin-coated in air (3500 rpm, 40 s) forming ∼35 nm films. After annealing the PEDOT:PSS at 150 °C for 30 min in air, the substrates were transferred into a glovebox under an inert atmosphere. Polymer/$PC_{71}BM$ (1:1 w/w in *o*-DCB) solutions were then spin-coated on top of the PEDOT:PSS layer at 2000 rpm for 60 s. The thickness of the active layer polymer/$PC_{71}BM$ films was ∼80−100 nm (KLA-TENCOR Alpha-Step IQ Surface Profiler). Finally, 15 nm of calcium and 100 nm of aluminum were thermally evaporated on the active layer under high vacuum (2×10^{-4} Pa) to complete the devices. The areas of the devices were 6 mm^2, as defined by the evaporator shadow mask area. Current−voltage (*J*−*V*) characteristics of the devices were measured under simulated AM1.5G irradiation (100 mW cm^{-2}) using a Xe lamp-based Newport 91160 300 W solar simulator. The light intensity was adjusted with an NREL-calibrated Si solar cell with a KG-5 filter. Device characteristics are reported as an average of at least four devices ± one standard deviation. Hole mobilities were extracted by fitting the current density−voltage curves using the Mott−Gurney relationship (space charge limited current) (SCLC) with a device structure of ITO/PEDOT:PSS/active layer/MoO_3/Ag.

4.6. GIWAXS Measurements. Grazing incidence wide-angle X-ray scattering (GIWAXS) characterization was performed at beamline 7.3.3, Advanced Light Source (ALS), Lawrence Berkeley National Lab (LBNL). X-ray energy was 10 keV and operated in top off mode. The scattering intensity was recorded on a 2D image plate (Pilatus 2M) with a pixel size of 172 μm (1475 × 1679 pixels). The samples were ∼15 mm long in the direction of the beam path, and the detector was located at a distance of 300 mm from the sample center (distance calibrated by AgB reference). The incidence angle was chosen to be 0.16° to optimize the signal-to-background ratio. Thin-film active layer blend samples were prepared on PEDOT:PSS covered Si wafers in a similar manner to the OPV devices, and pure polymer samples were prepared on Si wafers with a 2 nm natural oxide layer.

■ ASSOCIATED CONTENT

Supporting Information

The Supporting Information is available free of charge on the ACS Publications website at DOI: 10.1021/acs.macromol.6b00386.

Additional computational results for tetramer models, ^{1}H and ^{19}F NMR spectra for monomers and polymers, detailed MALDI-TOF spectra, UPS measurements and figures, 2D GIWAXS images for pure polymers and polymer/PCBM blends, and dark *J*−*V* curves for SCLC mobility (PDF)

■ AUTHOR INFORMATION

Corresponding Author

*(E.B.C.) E-mail: Coughlin@mail.pse.umass.edu.

Notes

The authors declare no competing financial interest.

■ ACKNOWLEDGMENTS

This work is supported as part of Polymer-Based Materials for Harvesting Solar Energy (PHaSE), an Energy Frontier Research Center funded by the U.S. Department of Energy, Office of Science, Office of Basic Energy Sciences, under Award DE-SC0001087. Support was also provided by the U.S. Office of Naval Research under contract N00014-15-1-2244, and by the Center for UMass/Industry Research on Polymers (CUMIRP) through Cluster E: Polymers for Renewable Energy. UPS experiments were performed in the UMass Center for Electronic Materials and Devices with the support of V. Duzhko. Mass spectral data for all materials were obtained at the University of Massachusetts Mass Spectrometry Center. J.D.H. acknowledges support from the National Science Foundation Graduate Research Fellowship Program (GRFP-1451512). The authors also acknowledge A. Hexemer and E. Schaible for support in ALS beamline 7.3.3. Portions of this research were performed at the Advanced Light Source, Lawrence Berkeley National Laboratory (LBNL), which is supported by the DOE, Office of Science, and Office of Basic Energy Sciences.

■ REFERENCES

(1) Yu, G.; Gao, J.; Hummelen, J. C.; Wudl, F.; Heeger, A. J. Polymer Photovoltaic Cells: Enhanced Efficiencies via a Network of Internal Donor-Acceptor Heterojunctions. *Science* **1995**, *270*, 1789−1791.

(2) Zhou, H.; Yang, L.; You, W. Rational Design of High Performance Conjugated Polymers for Organic Solar Cells. *Macromolecules* **2012**, *45*, 607−632.

(3) Service, R. F. Outlook Brightens for Plastic Solar Cells. *Science* **2011**, *332*, 293.

(4) Li, G.; Zhu, R.; Yang, Y. Polymer Solar Cells. *Nat. Photonics* **2012**, *6*, 153−161.

(5) Cheng, Y.-J.; Yang, S.-H.; Hsu, C.-S. Synthesis of Conjugated Polymers for Organic Solar Cell Applications. *Chem. Rev.* **2009**, *109*, 5868−5923.

(6) Guo, Y.; Yu, G.; Liu, Y. Functional Organic Field-Effect Transistors. *Adv. Mater.* **2010**, *22*, 4427−4447.

(7) Zhu, X.-H.; Peng, J.; Cao, Y.; Roncali, J. Solution-Processable Single-Material Molecular Emitters for Organic Light-Emitting Devices. *Chem. Soc. Rev.* **2011**, *40*, 3509−3524.

(8) Dang, M. T.; Hirsch, L.; Wantz, G. P3HT:PCBM, Best Seller in Polymer Photovoltaic Research. *Adv. Mater.* **2011**, *23*, 3597−3602.

(9) Marrocchi, A.; Lanari, D.; Facchetti, A.; Vaccaro, L. Poly(3-Hexylthiophene): Synthetic Methodologies and Properties in Bulk Heterojunction Solar Cells. *Energy Environ. Sci.* **2012**, *5*, 8457.

DOI: 10.1021/acs.macromol.6b00386
Macromolecules 2016, 49, 3028−3037

(10) Meyer, F. Fluorinated Conjugated Polymers in Organic Bulk Heterojunction Photovoltaic Solar Cells. *Prog. Polym. Sci.* **2015**, *47*, 70−91.
(11) Leclerc, N.; Chávez, P.; Ibraikulov, O.; Heiser, T.; Lévêque, P. Impact of Backbone Fluorination on π-Conjugated Polymers in Organic Photovoltaic Devices: A Review. *Polymers* **2016**, *8*, 11.
(12) Gohier, F.; Frère, P.; Roncali, J. 3-Fluoro-4-Hexylthiophene as a Building Block for Tuning the Electronic Properties of Conjugated Polythiophenes. *J. Org. Chem.* **2013**, *78*, 1497−1503.
(13) Koo, B.; Sletten, E. M.; Swager, T. M. Functionalized Poly(3-Hexylthiophene)s via Lithium−Bromine Exchange. *Macromolecules* **2015**, *48*, 229−235.
(14) Fei, Z.; Boufflet, P.; Wood, S.; Wade, J.; Moriarty, J.; Gann, E.; Ratcliff, E. L.; McNeill, C. R.; Sirringhaus, H.; Kim, J.-S.; Heeney, M. Influence of Backbone Fluorination in Regioregular Poly(3-Alkyl-4-Fluoro)thiophenes. *J. Am. Chem. Soc.* **2015**, *137*, 6866−6879.
(15) Kozycz, L. M.; Gao, D.; Seferos, D. S. Compositional Influence on the Regioregularity and Device Parameters of a Conjugated Statistical Copolymer. *Macromolecules* **2013**, *46*, 613−621.
(16) Yang, Y.-L.; Lee, Y.-H.; Lee, Y.-P.; Chiang, C.-J.; Shen, C.; Wu, C.-C.; Ohta, Y.; Yokozawa, T.; Dai, C.-A. Synthesis and Characterization of poly(3-Hexylthiophene)-poly(3-Hexyloxythiophene) Random Copolymers with Tunable Band Gap via Grignard Metathesis Polymerization. *Polym. Int.* **2014**, *63*, 2068−2075.
(17) Rudenko, A. E.; Khlyabich, P. P.; Thompson, B. C. Random Poly(3-Hexylthiophene- Co −3-Cyanothiophene) Copolymers via Direct Arylation Polymerization (DArP) for Organic Solar Cells with High Open-Circuit Voltage. *ACS Macro Lett.* **2014**, *3*, 387−392.
(18) Howard, J. B.; Noh, S.; Beier, A. E.; Thompson, B. C. Fine Tuning Surface Energy of Poly(3-Hexylthiophene) by Heteroatom Modification of the Alkyl Side Chains. *ACS Macro Lett.* **2015**, *4*, 725−730.
(19) Li, W.; Albrecht, S.; Yang, L.; Roland, S.; Tumbleston, J. R.; McAfee, T.; Yan, L.; Kelly, M. A.; Ade, H.; Neher, D.; You, W. Mobility-Controlled Performance of Thick Solar Cells Based on Fluorinated Copolymers. *J. Am. Chem. Soc.* **2014**, *136*, 15566−15576.
(20) He, X.; Mukherjee, S.; Watkins, S.; Chen, M.; Qin, T.; Thomsen, L.; Ade, H.; Mcneill, C. R. Influence of Fluorination and Molecular Weight on the Morphology and Performance of PTB7:PC 71 BM Solar Cells. *J. Phys. Chem. C* **2014**, *118*, 9918−9929.
(21) Wang, H.; Yu, X.; Yi, C.; Ren, H.; Liu, C.; Yang, Y.; Xiao, S.; Zheng, J.; Karim, A.; Cheng, S. Z. D.; Gong, X. Fine-Tuning of Fluorinated Thieno[3,4-B]thiophene Copolymer for Efficient Polymer Solar Cells. *J. Phys. Chem. C* **2013**, *117*, 4358−4363.
(22) Rudenko, A. E.; Wiley, C. A.; Stone, S. M.; Tannaci, J. F.; Thompson, B. C. Semi-Random P3HT Analogs via Direct Arylation Polymerization. *J. Polym. Sci., Part A: Polym. Chem.* **2012**, *50*, 3691−3697.
(23) Rudenko, A. E.; Latif, A. A.; Thompson, B. C. Influence of β-Linkages on the Morphology and Performance of DArP P3HT-PC61BM Solar Cells. *Nanotechnology* **2014**, *25*, 014005.
(24) Wang, Q.; Takita, R.; Kikuzaki, Y.; Ozawa, F. Palladium-Catalyzed Dehydrohalogenative Polycondensation of 2-Bromo-3-Hexylthiophene: An Efficient Approach to Head-to-Tail poly(3-Hexylthiophene). *J. Am. Chem. Soc.* **2010**, *132*, 11420−11421.
(25) Wang, Q.; Wakioka, M.; Ozawa, F. Synthesis of End-Capped Regioregular Poly(3-Hexylthiophene)s via Direct Arylation. *Macromol. Rapid Commun.* **2012**, *33*, 1203−1207.
(26) Mercier, L. G.; Leclerc, M. Direct (Hetero)Arylation: A New Tool for Polymer Chemists. *Acc. Chem. Res.* **2013**, *46*, 1597−1605.
(27) Rudenko, A. E.; Wiley, C. A.; Tannaci, J. F.; Thompson, B. C. Optimization of Direct Arylation Polymerization Conditions for the Synthesis of poly(3-Hexylthiophene). *J. Polym. Sci., Part A: Polym. Chem.* **2013**, *51*, 2660−2668.
(28) Rudenko, A. E.; Thompson, B. C. Optimization of Direct Arylation Polymerization (DArP) through the Identification and Control of Defects in Polymer Structure. *J. Polym. Sci., Part A: Polym. Chem.* **2015**, *53*, 135−147.
(29) Rudenko, A. E.; Thompson, B. C. Influence of the Carboxylic Acid Additive Structure on the Properties of Poly(3-Hexylthiophene) Prepared via Direct Arylation Polymerization (DArP). *Macromolecules* **2015**, *48*, 569−575.
(30) Okamoto, K.; Zhang, J.; Housekeeper, J. B.; Marder, S. R.; Luscombe, C. K. C−H Arylation Reaction: Atom Efficient and Greener Syntheses of π-Conjugated Small Molecules and Macromolecules for Organic Electronic Materials. *Macromolecules* **2013**, *46*, 8059−8078.
(31) Facchetti, A.; Vaccaro, L.; Marrocchi, A. Semiconducting Polymers Prepared by Direct Arylation Polycondensation. *Angew. Chem., Int. Ed.* **2012**, *51*, 3520−3523.
(32) *Gaussian 09, Revision D.01*: Frisch, M. J.; Trucks, G. W.; Schlegel, H. B.; Scuseria, G. E.; Robb, M. A.; Cheeseman, J. R.; Scalmani, G.; Barone, V.; Mennucci, B.; Petersson, G. A.; et al. Gaussian, Inc.: Wallingford, CT, 2013.
(33) Karpfen, A.; Choi, C. H.; Kertesz, M. Single-Bond Torsional Potentials in Conjugated Systems: A Comparison of Ab Initio and Density Functional Results. *J. Phys. Chem. A* **1997**, *101*, 7426−7433.
(34) Elmaci, N.; Yurtsever, E. Thermochromism in Oligothiophenes: The Role of the Internal Rotation. *J. Phys. Chem. A* **2002**, *106*, 11981−11986.
(35) Bongini, A.; Bottoni, A. A Theoretical Investigation of the Torsional Potential in 3,3′-Dimethyl-2,2′-Bithiophene and 3,4′-Dimethyl-2,2′-Bithiophene: A Comparison between HF, MP2, and DFT Theory. *J. Phys. Chem. A* **1999**, *103*, 6800−6804.
(36) Darling, S. B.; Sternberg, M. Importance of Side Chains and Backbone Length in Defect Modeling of poly(3-Alkylthiophenes). *J. Phys. Chem. B* **2009**, *113*, 6215−6218.
(37) Sakamoto, Y.; Komatsu, S.; Suzuki, T. Tetradecafluorosexithiophene: The First Perfluorinated Oligothiophene. *J. Am. Chem. Soc.* **2001**, *123*, 4643−4644.
(38) Palermo, E. F.; McNeil, A. J. Impact of Copolymer Sequence on Solid-State Properties for Random, Gradient and Block Copolymers Containing Thiophene and Selenophene. *Macromolecules* **2012**, *45* (15), 5948−5955.
(39) Hollinger, J.; Jahnke, A. A.; Coombs, N.; Seferos, D. S. Controlling Phase Separation and Optical Properties in Conjugated Polymers through Selenophene-Thiophene Copolymerization. *J. Am. Chem. Soc.* **2010**, *132*, 8546−8547.
(40) Chen, T.; Rieke, R. D. The First Regioregular Head-to-Tail Poly(3-Hexylthiophene-2,5-Diyl) and a Regiorandom Isopolymer: Ni vs Pd Catalysis of 2(5)-Bromo-5(2)-(bromozincio)-3-Hexylthiophene Polymerization. *J. Am. Chem. Soc.* **1992**, *114*, 10087−10088.
(41) Lombeck, F.; Komber, H.; Gorelsky, S. I.; Sommer, M. Identifying Homocouplings as Critical Side Reactions in Direct Arylation Polycondensation. *ACS Macro Lett.* **2014**, *3*, 819−823.
(42) De Winter, J.; Deshayes, G.; Boon, F.; Coulembier, O.; Dubois, P.; Gerbaux, P. MALDI-ToF Analysis of Polythiophene: Use of trans-2-[3-(4-t-Butyl-Phenyl)-2-Methyl-2-Propenylidene]malononitrile - DCTB - as Matrix. *J. Mass Spectrom.* **2011**, *46*, 237−246.
(43) Liang, Y.; Feng, D.; Wu, Y.; Tsai, S.; Li, G.; Ray, C.; Yu, L. Highly Efficient Solar Cell Polymers Developed via Fine-Tuning of Structural and Electronic Properties. *J. Am. Chem. Soc.* **2009**, *131*, 7792−7799.
(44) Zhang, M.; Guo, X.; Zhang, S.; Hou, J. Synergistic Effect of Fluorination on Molecular Energy Level Modulation in Highly Efficient Photovoltaic Polymers. *Adv. Mater.* **2014**, *26*, 1118−1123.
(45) Elumalai, N. K.; Uddin, A. Open Circuit Voltage of Organic Solar Cells: An in-Depth Review. *Energy Environ. Sci.* **2016**, *9*, 391−410.
(46) Khlyabich, P. P.; Rudenko, A. E.; Thompson, B. C. Random Poly(3-hexylthiophene-co-3-cyanothiophene) Copolymers with High Open-Circuit Voltage in Organic Solar Cells. *J. Polym. Sci., Part A: Polym. Chem.* **2014**, *52*, 1055−1058.

DOI: 10.1021/acs.macromol.6b00386
Macromolecules 2016, 49, 3028−3037